Ionic conduction, rectification, and selectivity in single conical nanopores

Javier Cervera
Departament de Ciències Experimentals, Universitat Jaume I, Apartado 224, E-12080 Castelló, Spain

Birgitta Schiedt and Reinhard Neumann
Gesellschaft für Schwerionenforschung (GSI), Planck Strasse 1, D-64291 Darmstadt, Germany

Salvador Mafé
Departament de Termodinàmica, Universitat de València, E-46100 Burjassot, Spain

Patricio Ramírez[a)]
Departament de Física Aplicada. Universitat Politècnica de València Camino de Vera s/n, E-46022 Valencia, Spain

Modern track-etching methods allow the preparation of membranes containing a single charged conical nanopore that shows high ionic permselectivity due to the electrical interactions of the surface pore charges with the mobile ions in the aqueous solution. The nanopore has potential applications in electrically assisted single-particle detection, analysis, and separation of biomolecules. We present a detailed theoretical and experimental account of the effects of pore radii and electrolyte concentration on the current-voltage and current-concentration curves. The physical model used is based on the Nernst-Planck and Poisson equations. Since the validity of continuum models for the description of ion transport under different voltages and concentrations is recognized as one of the main issues in the modeling of future applications, special attention is paid to the fundamental understanding of the electrical interactions between the nanopore fixed charges and the mobile charges confined in the reduced volume of the inside solution. © *2006 American Institute of Physics*. [DOI: 10.1063/1.2179797]

I. INTRODUCTION

Synthetic nanopores of dimensions comparable to the size of biological macromolecules such as proteins[1,2] and DNA (Refs. 3–5) have potential applications in single-particle detection, analysis, and separation of biomolecules. They are more robust and allow easier control of the geometry than biological channels, and can readily be integrated into functional systems.[3,6] Since most biomolecules in aqueous solutions are charged, a fundamental understanding of the electrical interactions between the nanopore fixed charges and the mobile charges confined in the small volume of the inside solution is needed. In particular, the validity of relatively simple continuum models for the description of ion transport under different voltages and concentrations has attracted attention recently,[3,4,7,8] and is generally recognized as one of the main issues in the modeling of future applications. Indeed, the transport problem involves typically (at least) three length scales: the biomolecule size, the nanopore dimensions, and the screening Debye length.[1,2,6,9] We will consider here, both theoretically and experimentally, the relative roles of the last two length scales for the case of conical nanopores obtained using the track-etching technique.[10–14]

Irradiation of polymer films such as polyethylene terephthalate (PET) with heavy ions and subsequent etching with alkali of the latent particle tracks allow the preparation of synthetic pores with diameters from few nanometers to the micrometer range.[10–17] As a result of the etching process, alkaline hydrolysis of ester bonds generates negative carboxyl groups (COO$^-$) fixed to the pore surface. When immersed in aqueous electrolyte solutions, the resulting charged membranes show ionic selectivity, favoring the passage of counterions (ions with charge opposite to that bound to the pores) but hindering the passage of coions (ions with charge of the same sign as that of the pores).

Modern one-side etching procedures make it possible to generate membranes containing only a *single* cylindrical, conical, or double conical nanopore.[10,13–17] These nanofluidic devices display properties that resemble those found in biological protein ion channels, such as ionic selectivity,[18,19] current rectification,[10,14–17,19,20] flux inhibition by protons and divalent cations,[13] transport of ions against concentration gradients,[21] and ion current fluctuations.[12] Therefore, synthetic track-etched nanopores have been proposed as model systems for the study of ion transport in biochannels.

Potential biotechnological applications of track-etched nanopores in the detection and analysis of single molecules (e.g., DNA chains) with a size comparable to the nanopore diameter have recently been reported by Siwy and co-workers,[19,20,22] In the experimental realizations, an applied electric field drives the charged molecules into the nanopore where they are detected as individual dips in ion current (a Coulter counter[23]) whose durations and shapes are related to the structure of the molecules. Also, a new particle detection method based on the electrophoretic capture and release of particles at the mouth of a conical nanopore has

---

a)Electronic mail: patraho@fis.upv.es

124, 104706-1

been proposed.[24] Recently, Martin and co-workers have developed a gold-plating technique that allowed them to control both the size and surface chemistry of cylindrical and conical track-etched nanopores.[25–31] The modification of the pore surface by chemisorption of different thiols or DNA chains permits the design of conical nanopores with unique ion transport and selectivity properties.[28,29,31]

The electrostatic interactions of mobile ions with the pore surface charges are responsible for the permselectivity of these nanostructures.[19,20,22,32–34] We have presented recently[9] a theoretical model for the ionic transport through synthetic conical nanopores. The model is based on the Poisson and Nernst-Planck (PNP) equations, and allows to calculate the profiles of electric potential and average concentration of mobile charge carriers along the pore. We present here a detailed theoretical and experimental account of the effects of pore radii and electrolyte concentration on the current versus voltage and current versus concentration curves. A comparison of the theory with experimental data for two PET conical nanopores provides new insights on the role of the electrostatic interactions in the ionic selectivity to cations and the observed conduction and rectification properties.

II. EXPERIMENT

The experimental data were obtained with PET polymer films (Hostaphan RN12, Hoechst, thickness of 12 μm). These films were irradiated at the UNILAC linear accelerator (GSI, Darmstadt) with single heavy ions (Au, U, or Pb) of an energy of 11.4 MeV per nucleon. Conical pores were created by etching the irradiated films from one side in a conductivity cell (9M NaOH) at room temperature, using a stopping solution (1M KCl+1M formic acid) on the opposite side of the membrane to neutralize the etchant in the pore tip immediately after the breakthrough (observed as a sudden occurrence of current through the pore[10]). To assure a nanometer-sized opening on the nonetched membrane side, the voltage used to monitor the etching process was applied in such a way that the active OH$^-$ ions were swept out of the pore.

We analyze the experimental results for two pores with radii of 3 and 22 nm (determined by conductivity measurements[10]) at the cone tip and of several hundred nanometers at the big aperture.

The current-voltage (I-V) curves were recorded under symmetric electrolyte conditions, using unbuffered KCl at pH 5.6±0.2 to avoid the introduction of additional ionic species into the system. The concentrations were varied from 3 down to 0.01M. The voltage was applied via Ag/AgCl electrodes with a National Instruments analog I/O card using a triangular signal of frequency of 0.005 Hz composed of 50 mV steps.

III. THEORY

Figure 1 shows schematically the polymeric film, containing a nanopore of thickness L, which separates two identical KCl solutions. The COO$^-$ groups generated by the track-etching process are assumed to be homogeneously distributed over the pore wall, with σ as the surface charge density. The pore radii at the left and right nanopore ends are
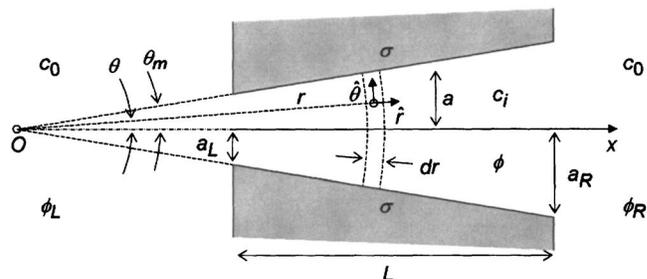

FIG. 1. Schematic view of the conical nanopore (not to scale) and the spherical coordinates with the origin in the cone apex O used for solving the PNP equations.

a_L and a_R, respectively, and θ_m is the pore opening angle [$\tan \theta_m = (a_R - a_L)/L$]. ϕ denotes the local dimensionless electric potential (1 unit corresponds to RT/F, where R, T, and F have their usual meaning[9]). c_i and ϕ_j refer to the concentration of species i ($i=+$ for cations and $i=-$ for anions) and the electric potential in the bulk of solution j ($j=L$ for the left solution and $j=R$ for the right solution), respectively. We assume that the external solutions are ideal and perfectly stirred. Also, electro-osmotic effects are ignored at a first approximation,[35] and the whole system is assumed to be isothermal.

The ionic transport through the nanopore is described by the Nernst-Planck equations,

$$\mathbf{J}_i = - D_i(\nabla c_i + z_i c_i \nabla \phi), \quad i = +,-, \tag{1}$$

together with the steady state continuity equations,

$$\nabla \cdot \mathbf{J}_i = 0, \quad i = +,-, \tag{2}$$

and the Poisson equation,

$$\nabla^2 \phi = \frac{F^2}{\varepsilon RT}(c_- - c_+). \tag{3}$$

In Eqs. (1)–(3) $\mathbf{J}_i$, D_i, and z_i are the flux, diffusion coefficient, and charge number of ionic species i, respectively, and ε is the dielectric permittivity of the pore solution.

Figure 1 shows the spherical coordinates, with the origin in the cone apex, used to solve Eqs. (1)–(3). In this coordinate system, Eqs. (1) and (3) take the following form:

$$-\frac{\mathbf{J}_i}{D_i} = \frac{\partial c_i}{\partial r}\hat{r} + \frac{1}{r}\frac{\partial c_i}{\partial \theta}\hat{\theta} + z_i c_i \left(\frac{\partial \phi}{\partial r}\hat{r} + \frac{1}{r}\frac{\partial \phi}{\partial \theta}\hat{\theta}\right), \quad i = +,-, \tag{4}$$

$$\frac{1}{r^2}\frac{\partial}{\partial r}\left(r^2 \frac{\partial \phi}{\partial r}\right) + \frac{1}{r^2 \sin \theta}\frac{\partial}{\partial \theta}\left(\sin \theta \frac{\partial \phi}{\partial \theta}\right) = \frac{F^2}{\varepsilon RT}(c_- - c_+). \tag{5}$$

We introduce now some approximations to solve the above equations. Since the pore angle is small, we assume that the ionic fluxes have only radial components,

$$\mathbf{J}_i = J_i \hat{r}, \quad i = +,-, \tag{6}$$

and Eq. (4) becomes

$$-\frac{J_i}{D_i} = \frac{\partial c_i}{\partial r} + z_i c_i \frac{\partial \phi}{\partial r}, \quad i = +,-. \tag{7}$$

Equation (6) is consistent with the boundary conditions for the ionic fluxes within the pore and establishes that the solution cannot penetrate the pore walls. Therefore $\hat{\theta} \cdot \mathbf{J}_i(r, \theta = \theta_m) = 0$, and the symmetry of the nanopore leads to $\hat{\theta} \cdot \mathbf{J}_i(r, \theta = 0) = 0$.

Instead of solving Eqs. (4) and (5) *locally*, we calculate *average* values over spherical shells with constant r and differential thickness dr limited by the border of the pore (see Fig. 1).[36] The average operator is defined as

$$\langle \rangle \equiv \frac{1}{(1 - \cos \theta_m)} \int_0^{\theta_m} d\theta \sin \theta. \tag{8}$$

This operator, applied to Eq. (7), gives

$$\langle J_i \rangle = -D_i \left(\frac{d\langle c_i \rangle}{dr} + z_i \langle c_i \rangle \frac{d\langle \phi \rangle}{dr} \right), \quad i = +,-, \tag{9}$$

where the averaged migration term can be written approximately as

$$\left\langle c_i \frac{\partial \phi}{\partial r} \right\rangle \approx \langle c_i \rangle \frac{d\langle \phi \rangle}{dr}, \quad i = +,-. \tag{10}$$

Since the system is at steady state, Eqs. (2) and (6) lead to

$$r^2 \langle J_i \rangle = \text{const}, \quad i = +,-, \tag{11}$$

and thus the total ionic flux through the pore cross section (defined as the spherical surface limited by the pore borders) is constant. From Eqs. (9) and (11),

$$\frac{d}{dr}(r^2 \langle J_i \rangle) = \frac{d}{dr}\left[-r^2 D_i \left(\frac{d\langle c_i \rangle}{dr} + z_i \langle c_i \rangle \frac{d\langle \phi \rangle}{dr} \right) \right] = 0, \quad i = +,-. \tag{12}$$

The average operator of Eq. (8) applied to Eq. (5) yields

$$\frac{1}{r^2}\frac{d}{dr}\left(r^2 \frac{d\langle \phi \rangle}{dr} \right) = \frac{F^2}{\varepsilon RT}(\langle c_- \rangle - \langle c_+ \rangle - X(r)), \tag{13}$$

since

$$\left\langle \frac{1}{r^2 \sin \theta} \frac{\partial}{\partial \theta}\left(\sin \theta \frac{\partial \phi}{\partial \theta} \right) \right\rangle$$
$$= \frac{\sin \theta_m}{r^2(1 - \cos \theta_m)} \left. \frac{\partial \phi}{\partial \theta} \right|_{\theta = \theta_m} = \frac{F^2 X(r)}{\varepsilon RT}, \tag{14}$$

where the Gauss law

$$\frac{1}{r} \left. \frac{\partial \phi}{\partial \theta} \right|_{\theta = \theta_m} = \frac{F\sigma}{\varepsilon RT} \tag{15}$$

has been used and

$$X(r) = \frac{\sin \theta_m \sigma}{Fr(1 - \cos \theta_m)} \tag{16}$$

is the fixed charge concentration (with its sign) contained in the differential spherical shell of radius r. Since $a = r \sin \theta_m$, Eq. (16) yields $X \approx 2\sigma/Fa$ for θ_m small, that is, the volume

fixed charge concentration contained in differential conical slabs of radius a.[37,38]

The boundary values for the average ionic concentrations and electric potential at the pore borders $r = r_L$ and $r = r_R$ are obtained assuming that the external and pore solution average concentrations are related through the Donnan equilibrium conditions,[39]

$$\langle c_i \rangle_L \equiv \langle c_i(r_L) \rangle = c_0 \exp\{-z_i \Delta\phi_{D,L}\}, \quad i = +,-, \tag{17}$$

$$\langle c_i \rangle_R \equiv \langle c_i(r_R) \rangle = c_0 \exp\{z_i \Delta\phi_{D,R}\}, \quad i = +,-, \tag{18}$$

where $\Delta\phi_{D,L} \equiv \langle \phi(r_L) \rangle - \phi_L$ and $\Delta\phi_{D,R} \equiv \phi_R - \langle \phi(r_R) \rangle$ are the Donnan potential drops at the left and right pore/external solution interfaces, respectively. Equations (17) and (18) assume that the ionic partition between the nanopore and the external solution is given by electrostatic interactions only.[39] The condition of local electroneutrality at these interfaces is

$$\sum_i z_i \langle c_i \rangle_j + X_j = 0, \quad j = L, R, \tag{19}$$

where $X_j \equiv X(r_j)$, and $j = L$ and R. Combining Eqs. (17) and (18) with Eq. (19), the average ionic concentrations and electric potentials at the pore/external solution interfaces are

$$\langle c_i \rangle_j \equiv \langle c_i(r_j) \rangle = \tfrac{1}{2}(-z_i X_j + \sqrt{X_j^2 + 4c_0^2}),$$
$$i = +,-; \quad j = L, R, \tag{20}$$

and

$$\langle \phi(r_j) \rangle = \phi_j - \frac{1}{z_i} \ln \frac{\langle c_i \rangle_j}{c_0}, \quad i = +,-; \quad j = L, R. \tag{21}$$

The I-V curve of the nanopore is obtained finally as follows. The average concentration and potential profiles at the applied voltage $V \equiv RT(\phi_L - \phi_R)/F$ are determined by integrating Eqs. (12) and (13) with the boundary conditions in Eqs. (20) and (21). The average ionic fluxes are then calculated from these profiles using Eq. (9). Finally,

$$I = 2\pi(1 - \cos \theta_m) r^2 \sum_i z_i F \langle J_i \rangle \tag{22}$$

is the total electric current passing through any spherical section of the nanopore (the usual sign convention is used: the current direction is that of cations). For θ_m small, the area of the spherical section in Eq. (22) reduces to πa^2.

IV. RESULTS AND DISCUSSION

Experimental I-V curves of single conical PET nanopores measured under symmetric electrolyte conditions are shown in Figs. 2(a) and 2(b). Figure 2(a) corresponds to sample 1 ($a_L = 22$ nm, $a_R = 168$ nm, and $\theta_m = 0.7°$) and Fig. 2(b) to sample 2 ($a_L = 3$ nm, $a_R = 220$ nm, and $\theta_m = 1°$). The curves were recorded at room temperature ($T = 293$ K) and are parametric in the external KCl concentration c_0. Voltages were applied on the narrow side of the pore, with the other side connected to ground (0 V), and currents $I > 0$ flowing from the narrow opening towards the wide opening of the pore. Clearly, the two samples exhibit rectification phenomena, with high ($V > 0$) and low ($V < 0$) conducting states for
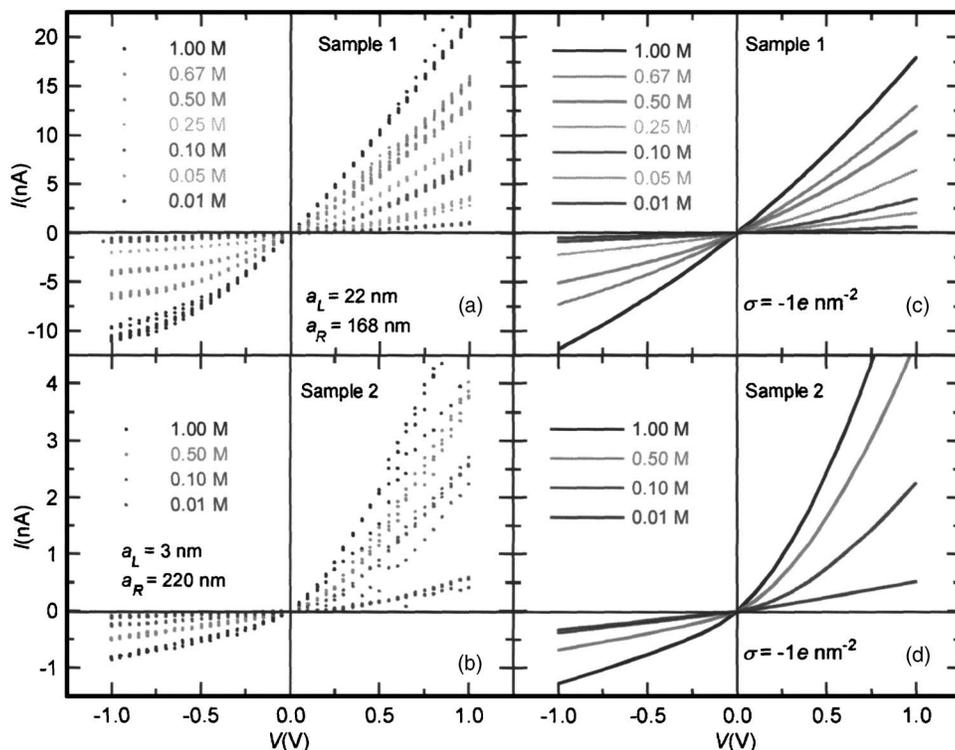
FIG. 2. Experimental *I-V* curves for samples 1(a) and 2(b). Theoretical *I-V* curves for samples 1(c) and 2(d).

all electrolyte concentrations. At a given voltage, the current increases with the electrolyte concentration. A comparison of the curves for the two samples shows that the current is determined by the small pore radius [note the different vertical scales in Figs. 2(a) and 2(b)]. The theoretical results for $\varepsilon = 80\varepsilon_0$, where ε_0 is the electric permittivity of vacuum, and the (infinite dilution) diffusion coefficients[40] $D_+ = 1.95 \times 10^{-5}$ cm^2/s and $D_- = 2.03 \times 10^{-5}$ cm^2/s are shown in Figs. 2(c) and 2(d). The only free parameter of the model (the surface charge density) is assumed to be $\sigma = -1$ e/nm^2 for the two samples, where e is the elementary charge, which is within the range of the experimental values reported for cylindrical and conical PET nanopores.[14] In spite of the different pore radii of the samples and the wide range of electrolyte concentrations used, the theoretical results show a reasonable agreement with the experimental data. The discrepancies between theory and experiments are partly due to the uncertainties in the determination of the pore radii and the surface charge density. Small changes in these values can improve further the agreement between theory and experiment but we wish to analyze here the qualitative trends rather than to present quantitative fittings. Other effects not included in the model are the following. First, the shape of the nanopore might not be exactly conical[29,31] (the region of the small opening determines the *I-V* characteristics of the nanopores, as we will see later). Second, the surface charge density could not be homogeneous, as assumed in the model. Third, the diffusion boundary layers at the membrane/solution interfaces could lead to extra potential drops not included in the model. Fourth, the diffusion coefficients of the ionic species in the nanopore could be lower than those in the bulk of the surrounding solutions.[41,42] Finally, the approximation made in Eq. (10) requires further discussion.

Since $c_i > 0$ ($i = +$ and $-$) and $\partial\phi/\partial r$ is not expected to change its sign once the characteristic model parameters have been set, the Schwarz inequality

$$\left| \left\langle c_i \frac{\partial\phi}{\partial r} \right\rangle \right| \leq |\langle c_i \rangle| \left| \frac{d\langle\phi\rangle}{dr} \right| \tag{23}$$

points out that the theoretical model tends to overestimate the ionic average fluxes. Therefore, the real current could be lower than that calculated using Eq. (22).

To allow a more detailed interpretation of the experiments in Fig. 2, we have calculated the profiles of average concentrations and electrical potential versus the coordinate x along the pore symmetry axis. The curves in Fig. 3, obtained with $c_0 = 0.1M$, are parametric in the applied voltage V. The theoretical curves on the left correspond to the average electric potential profile [Fig. 3(a)] and the average concentration profiles of majority [Fig. 3(b)] and minority [Fig. 3(c)] ions for sample 1. The curves on the right [Figs. 3(d)–3(f)] correspond also to the above profiles but now calculated for sample 2. The electric potential profiles are strongly nonlinear in the region of the pore tip, where the effects of the fixed charges are more noticeable. The insets in Figs. 3(a) and 3(d) show a clear potential well at the pore tip in both samples.[9,18] As a result, major changes in the electric field and ion concentrations occur within this region. For $V > 0$ the electric field drags the majority ions to the pore tip, where these ions tend to accumulate due to the fixed charges, and this leads to a maximum in the concentration profile. The minority ions are also forced towards the nanopore tip in order to preserve electroneutrality, and the shape of the corresponding concentration profile is similar to that of the majority ions. Consequently, the concentration of charge carriers increases with the potential difference V, i.e., with the
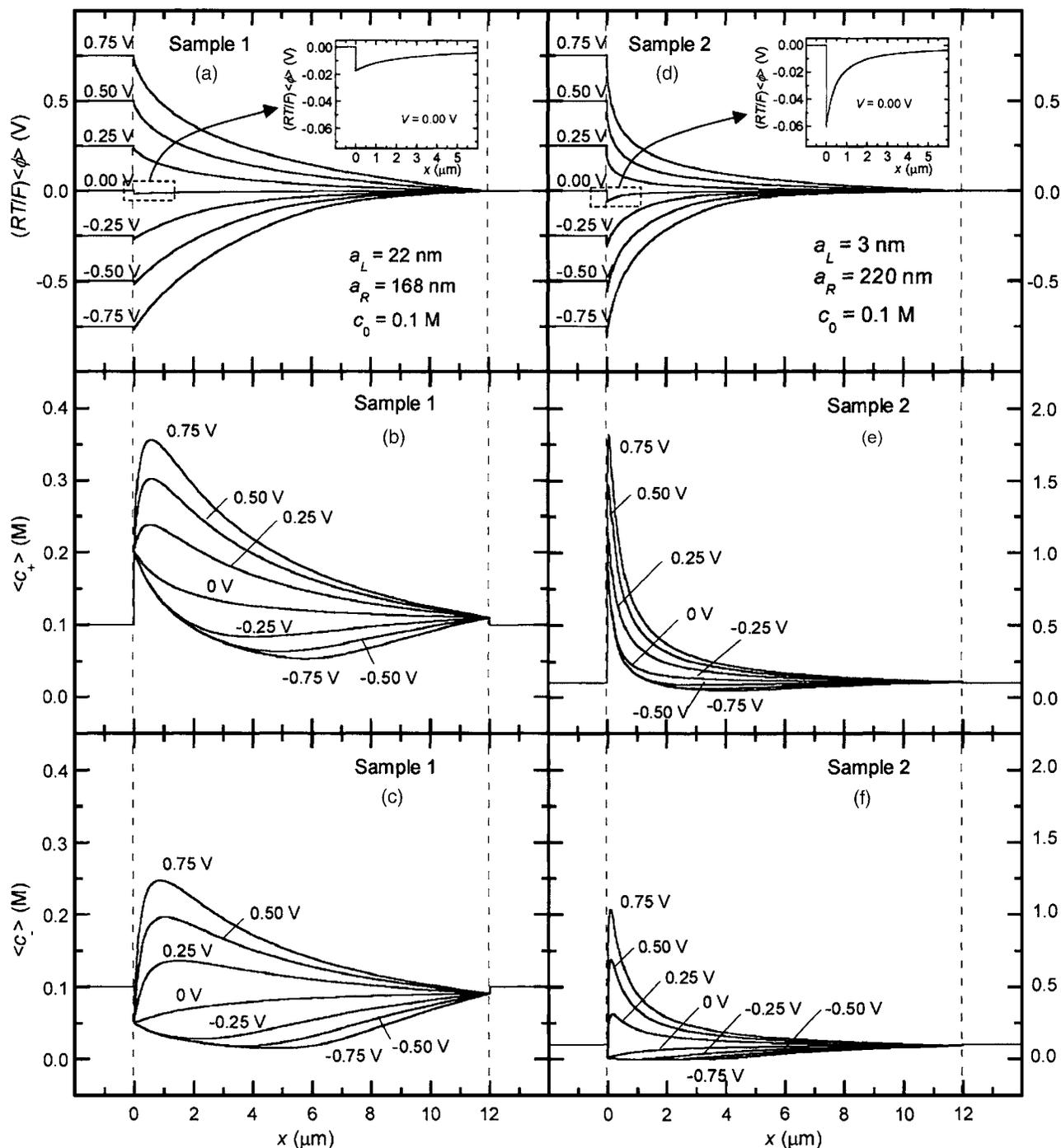
FIG. 3. Calculated average profiles of the electric potential and the concentrations of majority and minority mobile ions for samples 1[(a)–(c)] and 2[(d)–(f)]. The curves are parametric in V.

strength of the electric field that drags the majority carriers to the tip region. Since the conductance of the nanopore (the derivative of I with respect to V) is roughly proportional to the concentration of charge carriers, I increases rapidly with V (see the I-V curves of Fig. 2 for $V > 0$). For $V < 0$, however, the electric field drives the majority ions out of the narrow pore region, and the minority ions follow the same trend to preserve electroneutrality (the concentration profiles of both the majority and minority ions attain now a minimum). The decreased concentrations of charge carriers give lower conductances than in the case $V > 0$ (see Fig. 3), and

an almost linear increase of I with V occurs. This is due to the limited amount of mobile ions present now in the tip region. Note also that the ionic depletion in this region decreases the Debye screening of the nanopore fixed charges that oppose the effect of the applied electric field when $V < 0$. Ionic depletion leads to a decreased concentration of mobile charges and, in turn, to a (locally) high Debye length. Therefore, the Debye screening is decreased in the sense that larger distances are now needed to electrostatically screen the nanopore fixed charges.

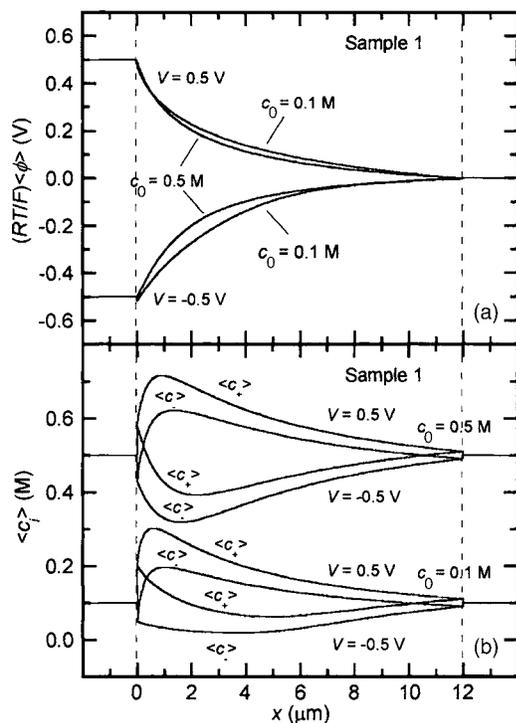A comparison of the average profiles for the two samples

FIG. 4. Calculated average profiles of electric potential (a) Concentrations of majority and minority mobile ions (b) at $V=0.5$ and -0.5 V for sample 1. The curves are parametric in c_0.

FIG. 5. Calculated ratio of the current transported by cations (I_+) to the total current (I) vs V for sample 2(a). The curves are parametric in c_0 and constitute a measure of the selectivity of the pore. Comparative of the above ratio for the two samples at $c_0=0.1M$ and $c_0=1M$ (b).

shows that the nonlinearity of the electric potential profile [Figs. 3(a) and 3(d)] is more noticeable in sample 2 (a_L =3 nm) than in sample 1 (a_L=22 nm). The effects of the fixed charges and the electric field on the average concentration profiles are therefore more pronounced in sample 2 than in sample 1 [compare Figs. 3(e) and 3(f) with Figs. 3(b) and 3(c); note the different scales in the vertical axes]. This confirms further the assumption that the *I-V* characteristics of the nanopore are dictated by the interaction of the mobile carriers with the fixed charges in the pore tip region. Therefore, small changes in the size and shape of this region can result in significant changes in the ionic transport properties of the nanopore, making ionic conduction and selectivity modulation feasible.

Figure 4 shows the average electric potential [Fig. 4(a)] and concentration profiles [Fig. 4(b)] calculated for sample 1 at $V=+0.5$ V and $V=-0.5$ V with $c_0=0.1$ and $0.5M$ (similar curves could also be obtained for sample 2). The external electrolyte concentration does not change qualitatively the average electric potential profile, although the increase in the number of charge carriers with c_0 leads to the increase of the electric current shown in the experiments of Fig. 2. The average ionic concentration profiles of Figs. 3 and 4 show that, at a given V, the difference in the ionic concentrations depends on the coordinate x along the pore axis, attaining a maximum at the cone tip region where the volume fixed charge density is higher. Therefore, the selectivity of the pore to cations varies locally in the conical nanopores. To quantify the selectivity of the whole pore to cations, we have calculated the fraction of the total current transported by these ions $|I_+/I|$ where
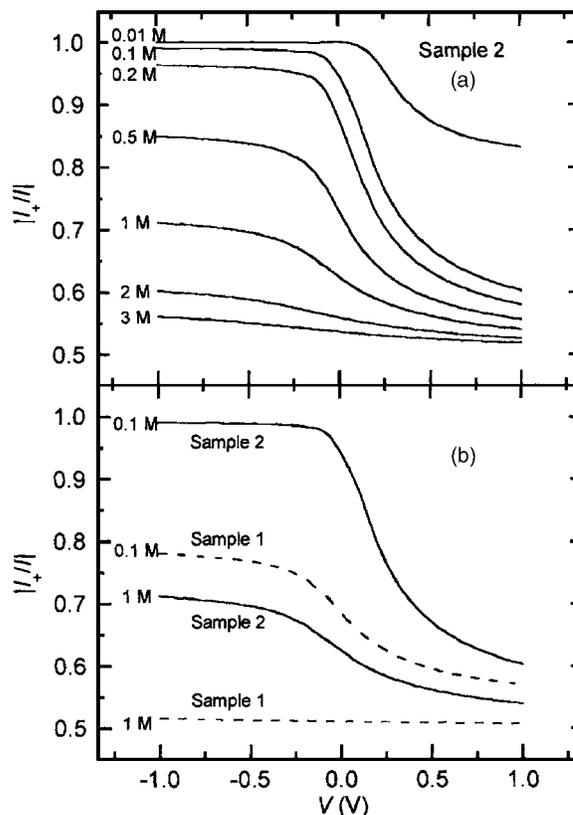
$$I_+ = 2\pi(1 - \cos\theta_m)r^2 z_+ F\langle J_+\rangle. \tag{24}$$

Figure 5(a) shows the $|I_+/I|$ versus V curves for sample 2 parametrically in c_0. The selectivity of the nanopore to cations is higher for $V<0$ than that for $V>0$, regardless of the electrolyte concentration. As could be expected, the selectivity of the nanopore to cations decreases with increasing c_0 at a given V. For the lowest electrolyte concentration c_0 $=0.01M$, $|I_+/I|\approx 1$ for $V=-1$ V and $|I_+/I|\approx 0.83$ for V $=1$ V. At the highest electrolyte concentration $c_0=3M$, $|I_+/I|\approx 0.56$ for $V=-1$ V and $|I_+/I|\approx 0.52$ for $V=1$ V. The decrease of $|I_+/I|$, when V changes from negative to positive values (and also when the electrolyte concentration is increased), occurs because of the high concentrations of mobile ions inside the pore shielding the effect of the fixed negative charges, responsible for the selectivity to cations. Figure 5(b) allows us to compare the calculated values of $|I_+/I|$ for samples 1 and 2: The selectivity to cations is higher in sample 2 than in sample 1 because the effects of fixed charges are more pronounced for the case of the nanopore with the smaller radius of the pore tip.

A measure of the rectification effect in conical nanopores is the ratio $|I(V)/I(-V)|$.[17,20] Figure 6 shows the above rectification ratio versus c_0 for samples 1 and 2 with $V=0.5$ V. The points correspond to the experimental data and the curves to the theoretical results (plots obtained at other voltages show similar characteristics as those in Fig. 6). The experimental rectification ratios increase rapidly for low c_0,
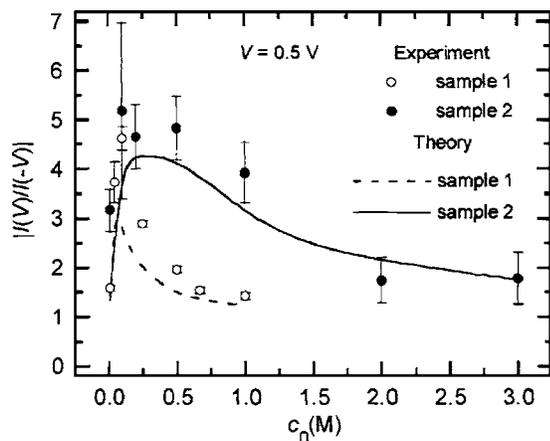
FIG. 6. Rectification ratio vs c_0 for samples 1 and 2 at $V=0.5$ V. The points correspond to the experimental data and the continuous lines to the theoretical results.

attain a maximum at $c_0 \approx 0.1M$, and then decrease for $c_0 > 0.1M$. The rectification ratio of sample 2 is higher than that of sample 1 over the whole concentration range. The theoretical curves follow qualitatively these experimental trends, reproducing clearly the observed maxima at $c_0 \approx 0.1M$, although the model underestimates the rectification ratio for the two nanopores. Again, the theoretical results are very sensitive to the pore radii and the surface charge density used in the calculations, and a detailed knowledge of the size and shape of the nanopore tip is necessary for more quantitative fittings.

To better understand the maxima in Fig. 6, we have calculated $|I(V)|$ and $|I(-V)|$ versus c_0 for $V=0.5$ V in the case of sample 2 (see Fig. 7). Both the experimental points and the theoretical curves show that $|I(V)|$ and $|I(-V)|$ tend to the same limiting value when $c_0 \rightarrow 0$, giving $|I(V)/I(-V)| \approx 1$ at low concentrations. This can be explained using the above theoretical model. In the limit $c_0 \rightarrow 0$, the calculated profiles for the average ion concentrations show total coion exclusion from the nanopore, and therefore

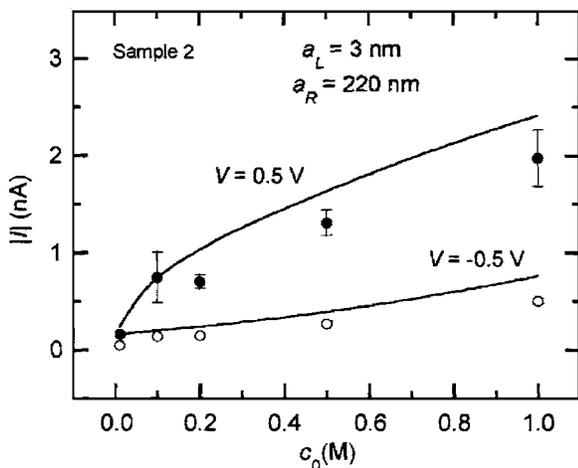$$\langle c_- \rangle \ll \langle c_+ \rangle \approx -X(r), \quad (25)$$

FIG. 7. Absolute value of the total electric current vs c_0 for sample 2 at $V=0.5$ V and $V=-0.5$ V. The points correspond to the experimental data and the continuous lines to the theoretical results.

$$r^2 \langle J_- \rangle \ll r^2 \langle J_+ \rangle = \text{const.} \quad (26)$$

Integration of Eq. (12) for $i=+$ gives then

$$r^2 \langle J_+ \rangle \approx D_+ \frac{\sin\theta_m \sigma}{F(1-\cos\theta_m)} \left[\frac{\langle \phi \rangle_R - \langle \phi \rangle_L}{\ln(a_R/a_L)} - 1 \right], \quad (27)$$

where the average potential drop through the nanopore is

$$\langle \phi \rangle_R - \langle \phi \rangle_L = -\Delta\phi_{D,L} - \Delta\phi_{D,R} - \frac{FV}{RT} \approx \ln(a_R/a_L) - \frac{FV}{RT}, \quad (28)$$

and the Donnan potential drops $\Delta\phi_{D,j}$ $(j=L,R)$ have been calculated from Eqs. (17) and (18) assuming that

$$\langle c_+ \rangle_j \approx -X(r_j), \quad j=L,R. \quad (29)$$

Finally, the I-V curve yields the following linear relationship:

$$I \approx 2\pi(1-\cos\theta_m)Fr^2\langle J_+ \rangle \approx -\frac{2\pi D_+ \sin\theta_m F\sigma}{RT\ln(a_R/a_L)}V, \quad (30)$$

that gives $|I(V)/I(-V)| \approx 1$ regardless of the pore radii, in agreement with the experimental data in Fig. 7. Also, the derivative of the rectification ratio $|I(V)/I(-V)|$ with respect to c_0 is

$$\frac{d|I(V)/I(-V)|}{dc_0} = \frac{|I(-V)|(d|I(V)|/dc_0) - |I(V)|(d|I(-V)|/dc_0)}{|I(-V)|^2}, \quad (31)$$

where $d|I(V)|/dc_0 > 0$ and $d|I(-V)|/dc_0 > 0$. Figure 7 reveals that, for low concentrations, $d|I(V)|/dc_0 \gg d|I(-V)|/dc_0$, and, although $|I(V)| > |I(-V)|$, Eq. (31) takes positive values. Therefore, the net result is an increase of $|I(V)/I(-V)|$ with c_0, in agreement with the experimental data of Fig. 6. On the contrary, for $c_0 > 0.1M$, $d|I(V)|/dc_0 > d|I(-V)|/dc_0$, while $|I(V)| \gg |I(-V)|$. Equation (31) takes then negative values, and the ratio $|I(V)/I(-V)|$ decreases with c_0 accordingly (see Fig. 6).

Figure 8 shows the dependence of the electric current with the concentration of the external electrolyte for samples 1 and 2. The curves are parametric in V. The dashed lines are drawn to guide the eyes through the experimental points in Figs. 8(a) (sample 1) and 8(b) (sample 2). The theoretical results of Figs. 8(c) (sample 1) and 8(d) (sample 2) follow the experimental trends over the whole range of applied voltages and electrolyte concentrations. The absolute value of I increases monotonically with c_0, although this increase depends on the polarity of the applied voltage: For $V>0$ the increase is more pronounced than for $V<0$. This is explained by the significant increase of the carrier concentrations obtained with $V>0$ compared with the case $V<0$ (see Fig. 3). Also, at a fixed concentration, the difference in the currents between two consecutive curves is higher for $V>0$ than for $V<0$ in both samples, as could be anticipated from the average profiles in Figs. 3(a), 3(b), 3(d), and 3(e). Therefore, we see again that the theoretical results of Figs. 3 and 4 reflecting the electrical interactions between the nanopore fixed charges and the mobile charges allow to rationalize the experimental data.
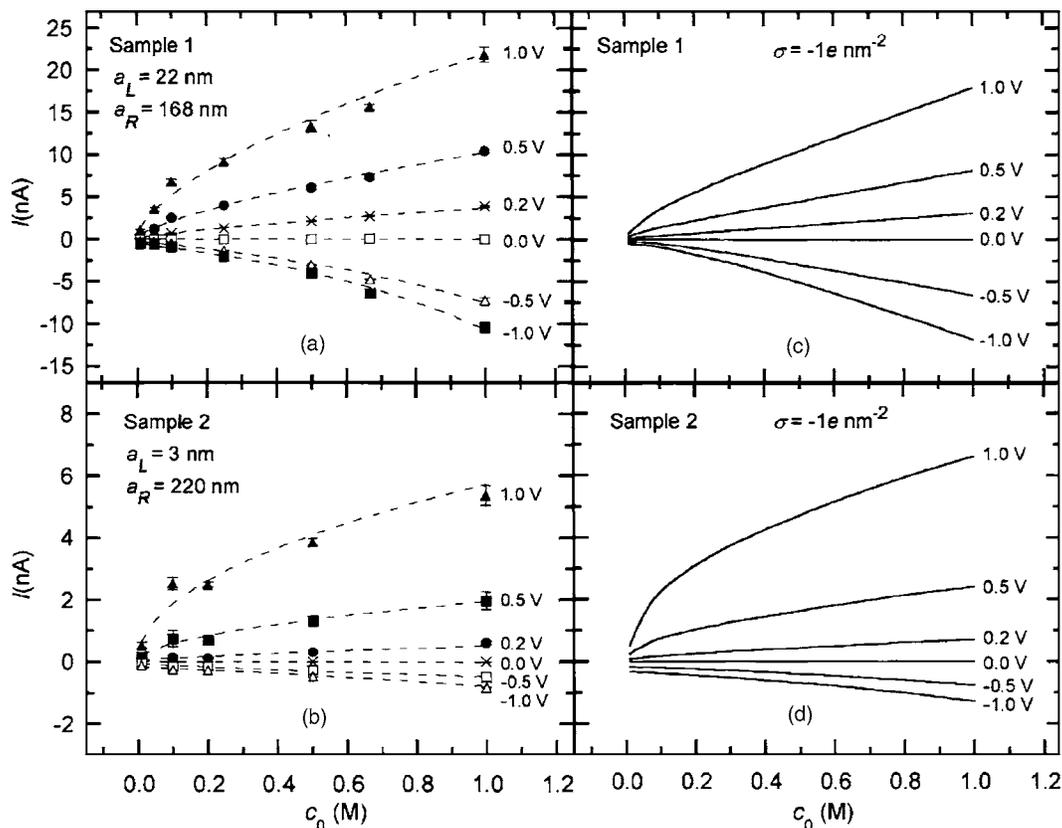
FIG. 8. Electric current vs concentration of the external electrolyte for samples 1 and 2. The curves are parametric in *V*. Experimental results for samples 1(a) and 2(b). Theoretical results for samples 1(c) and 2(d). The dashed lines in (a) and (b) are drawn to guide the eyes.

V. CONCLUSIONS

We have described the ionic conduction and selectivity properties of two PET conical nanopores with different pore radii on the basis of the experimental *I-V* curves obtained at different concentrations. The experimental data have been interpreted in terms of a theoretical model based on the PNP equations. The model considers the surface charge density of the nanopore as the only fitting parameter and allows the calculation of the average ionic concentration and electric potential profiles within the pore. The shape of these profiles offers simple explanations for the electrical phenomena observed. In particular, the mechanisms underlying current rectification and pore selectivity to cations, as well as the changes observed in the nanopore transport properties with the external electrolyte concentration, have been elucidated introducing a reduced number of basic concepts. The electrostatic interaction of the mobile ions with the nanopore surface charges appears to be largely responsible for the transport phenomena observed. This interaction can be approximately described with a relatively simple continuum model, probably because the nanopore radii are larger than the screening Debye length over most of the experimental concentration range considered (note also that these radii are also much greater than the typical ion size).

[1] K.-Y. Chun and P. Stroeve, Langmuir **18**, 4653 (2002).
[2] J.-R. Ku and P. Stroeve, Langmuir **20**, 2030 (2004).
[3] R. Fan, R. Karnik, M. Yue, D. Li, A. Majumdar, and P. Yang, Nano Lett. **5**, 1633 (2005).
[4] D. Fologea, J. Uplinger, B. Thomas, D. S. Mcnabb, and J. Li, Nano Lett. **5**, 1734 (2005).
[5] A. J. Storm, J. H. Chen, H. W. Zandbergen, and C. Dekker, Phys. Rev. E **71**, 051903 (2005).
[6] R. Karnik, K. Castelino, R. Fan, P. Yang, and A. Majumdar, Nano Lett. **5**, 1638 (2005).
[7] A. Fuliński, I. D. Kosińska, and Z. Siwy, Europhys. Lett. **67**, 683 (2004).
[8] H. Daiguji, Y. Oka, and K. Shirono, Nano Lett. **5**, 2274 (2005).
[9] J. Cervera, B. Schiedt, and P. Ramírez, Europhys. Lett. **71**, 35 (2005).
[10] P. Y. Apel, Y. E. Korchev, Z. Siwy, R. Spohr, and M. Yoshida, Nucl. Instrum. Methods Phys. Res. B **184**, 337 (2001).
[11] C. L. Bashford, G. M. Alder, and C. A. Pasternak, Biophys. J. **82**, 2032 (2002).
[12] Y. E. Korchev, C. L. Bashford, G. M. Alder, P. Y. Apel, D. T. Edmonds, A. A. Lev, K. Nandi, A. V. Zima, and C. A. Pasternak, FASEB J. **11**, 600 (1997).
[13] A. A. Lev, Y. E. Korchev, T. K. Rostovtseva, C. L. Bashford, D. T. Edmonds, and C. A. Pasternak, Proc. R. Soc. London, Ser. B **252**, 187 (1993).
[14] Z. Siwy, Y. Gu, H. A. Spohr, D. Baur, A. Wolf-Reber, R. Spohr, P. Apel, and Y. E. Korchev, Europhys. Lett. **60**, 349 (2002).
[15] Z. Siwy, P. Apel, D. Dobrev, R. Neumann, R. Spohr, C. Trautmann, and K. Voss, Nucl. Instrum. Methods Phys. Res. B **208**, 143 (2003).
[16] Z. Siwy, D. Dobrev, R. Neumann, C. Trautmann, and K. Voss, Appl. Phys. A: Mater. Sci. Process. **76**, 781 (2003).
[17] Z. Siwy, P. Apel, D. Baur, D. D. Dobrev, Y. E. Korchev, R. Neumann, R. Spohr, C. Trautmann, and K. O. Voss, Surf. Sci. **532–535**, 1061 (2003).
[18] Z. Siwy and A. Fuliński, Am. J. Phys. **72**, 567 (2004).

[19] Z. Siwy, I. D. Kosińska, A. Fuliński, and C. R. Martin, Phys. Rev. Lett. **94**, 048102 (2005).

[20] B. Schiedt, K. Healy, A. P. Morrison, R. Neumann, and Z. Siwy, Nucl. Instrum. Methods Phys. Res. B **236**, 109 (2005).

[21] Z. Siwy and A. Fuliński, Phys. Rev. Lett. **89**, 198103 (2002).

[22] A. Mara, Z. Siwy, C. Trautmann, J. Wan, and F. Kamme, Nano Lett. **4**, 497 (2004).

[23] R. W. DeBlois and C. P. Bean, Rev. Sci. Instrum. **41**, 909 (1970).

[24] S. Lee, Y. Zhang, H. S. White, C. C. Harrel, and C. R. Martin, Anal. Chem. **76**, 6108 (2004).

[25] C. R. Martin, Science **266**, 1961 (1994).

[26] M. Nishizawa, V. P. Menon, and C. R. Martin, Science **268**, 700 (1995).

[27] C. R. Martin, M. Nishizawa, K. B. Jirage, and M. Kang, J. Phys. Chem. B **105**, 1925 (2001).

[28] Z. Siwy, E. Heins, C. C. Harrell, P. Kohli, and C. R. Martin, J. Am. Chem. Soc. **126**, 10850 (2004).

[29] C. C. Harrell, P. Kohli, Z. Siwy, and C. R. Martin, J. Am. Chem. Soc. **126**, 15646 (2004).

[30] C. C. Harrell, S. B. Lee, and C. R. Martin, Anal. Chem. **75**, 6861 (2003).

[31] N. Li, S. Yu, C. C. Harrell, and C. R. Martin, Anal. Chem. **76**, 2025 (2004).

[32] D. Woermann, Nucl. Instrum. Methods Phys. Res. B **194**, 458 (2002).

[33] D. Woermann, Phys. Chem. Chem. Phys. **5**, 1853 (2003).

[34] D. Woermann, Phys. Chem. Chem. Phys. **6**, 3130 (2004).

[35] T. K. Rostovtseva, C. L. Bashford, G. M. Alder, G. N. Hill, C. McGiffert, P. Y. Apel, G. Lowe, and C. A. Pasternak, J. Membr. Biol. **151**, 29 (1996).

[36] E. H. Cwirko and R. G. Carbonell, J. Colloid Interface Sci. **129**, 513 (1989).

[37] P. Ramírez, S. Mafé, V. M. Aguilella, and A. Alcaraz, Phys. Rev. E **68**, 011910 (2003).

[38] P. Ramírez, S. Mafé, A. Alcaraz, and J. Cervera, J. Phys. Chem. B **107**, 13178 (2003).

[39] N. Lakshminarayanaiah, *Equations of Membrane Biophysics* (Academic, New York, 1984).

[40] R. A. Robinson and R. H. Stokes, *Electrolyte Solutions* (Butterworth, London, 1955).

[41] G. M. Pauletti, F. W. Okumu, and R. T. Borchardt, Pharm. Res. **14**, 164 (1997).

[42] G. B. Benedek and F. M. H. Villars, *Physics with Illustrative Examples from Medicine and Biology (Statistical Physics)* (Springer-Verlag, Heidelberg, 2000).